Chinese Journal of
POLYMER SCIENCE

RESEARCH ARTICLE

https://doi.org/10.1007/s10118-026-3604-y
Chinese J. Polym. Sci. **2026**, *44*, 1843–1854

Real-Time Monitoring of Component Conversion during the Foaming and Curing Process of Self-expanding Polyurethane Grouts

Xiao-Long Li, Xuan-Xuan Zi, Xiao-Feng Liu*, Ming Guo, Yan-Hui Zhong, and Bei Zhang

School of Water Conservancy and Transportation, Zhengzhou University, Zhengzhou 450001, China

Abstract Polyurethane polymer grouting materials with rapid expansion and solidification characteristics have been widely applied for infrastructure repair and reinforcement. An accurate characterization of the chemical reaction process of the slurry is essential for investigating its grouting mechanism. However, the high concentration of isocyanate groups in such polymer systems causes a "flat-top phenomenon" in Fourier transform infrared (FTIR) spectroscopy, rendering it difficult to accurately determine the conversion rate. To address this issue, a real-time method for measuring the reaction conversion rates of slurry components was proposed. The polyol conversion rate was obtained by tracking the integral area changes of the C—O bond peak in the carbamate product relative to the internal standard. The total slurry volume was determined at different time intervals using light detection and ranging (LiDAR)-based point cloud scanning, from which the gas volume was estimated. Combined with the solubility curve of the physical blowing agent and ideal gas law, the conversion rate of the chemical blowing agent was calculated. The isocyanate conversion rate was indirectly inferred based on the measured polyol and chemical blowing agent conversions. This method was applied to a polyurethane grouting material used in an engineering project, and the time-resolved conversion curves of all components throughout the reaction were obtained. The results revealed a three-stage evolution: a slow initial increase, a rapid rise in the middle stage, and a gradual deceleration in the later stage. The foaming reaction proceeded consistently faster than the gelation reaction did. These findings provide a foundation for further research on the diffusion mechanisms of polyurethane polymer slurries.

Keywords Grouting materials; Polymer; Chemical reaction; Component conversion rate testing

Citation: Li, X. L.; Zi, X. X.; Liu, X. F.; Guo, M.; Zhong, Y. H.; Zhang, B. Real-time monitoring of component conversion during the foaming and curing process of self-expanding polyurethane grouts. *Chinese J. Polym. Sci.* **2026**, *44*, 1843–1854.

INTRODUCTION

In recent years, polyurethane-based grouting materials with self-expanding properties have attracted significant attention in the field of injection grouting owing to their rapid curing, high expansion ratio, excellent water resistance, early strength development, and mechanical toughness.[1] These materials have been widely employed in sand reinforcement, road void filling, and dam seepage control projects.[2–4] As a chemically reactive system, the expansion and solidification processes of polyurethane slurries are governed by complex reaction kinetics, which directly influence the slurry diffusion, foam structure development, and overall engineering performance. Therefore, accurate characterization of the chemical reaction process is essential for understanding the diffusion behavior and optimizing grouting strategies.

Various thermal and rheological techniques have been employed to investigate the kinetic behavior of polyurethane systems. An adiabatic temperature rise method was employed to study the rapid curing process of polyurethane systems, as reported by Lipshitz and Macosko.[5] By monitoring the temperature increase during the reaction, they applied the least-squares method to fit the kinetic models and extract key parameters, such as the pre-exponential factor and activation energy. Kamal *et al*.[6] utilized differential scanning calorimetry (DSC) to record the exothermic behavior during thermosetting resin curing and proposed an autocatalytic model. By fitting the relationship between the heat release rate and conversion, the rate constant and kinetic parameters describing the polymerization of the slurry were obtained. Dimier *et al*.[7] combined DSC with rheological testing to monitor exothermic behavior and viscosity changes during isocyanate curing, establishing a three-step kinetic model to simulate the entire curing process. They further identified the gel point by the crossover of dynamic moduli, achieving simultaneous characterization of thermal and rheological behaviors. Li *et al*.[8,9] solved the rate equations using the fourth-order Runge-Kutta algorithm based on kinetic parameters and reaction rate equations to generate time-conversion profiles of polyurethane curing and foaming reactions. However, most of the above studies rely on indirect parameter inversion and numerical simulations, which lack direct experimental measurements of reactant conversion rates, thereby limiting the accuracy of the kinetic modeling and simulation results.

* Corresponding author, E-mail: lxf1997@zzu.edu.cn
Received December 16, 2025; Accepted January 29, 2026; Published online May 20, 2026

Traditional experimental techniques for characterizing polyurethane reactions mainly focus on determining the reactive isocyanate group (—NCO) content *via* chemical or instrumental analysis.[10–13] Among chemical methods, the most commonly used technique is toluene-dibutylamine titration, which determines the —NCO content *via* a nucleophilic addition reaction that consumes dibutylamine, followed by titration of the residual amine.[14] However, this method requires large volumes of solvents, poses environmental concerns, and incurs high analytical costs. By contrast, instrumental techniques offer greater precision and operational convenience. For example, Chen *et al.*[15] established a quantitative method for determining the free —NCO content in prepolymers using high-performance liquid chromatography (HPLC) combined with derivatization, demonstrating good linearity and stability. Wu *et al.*[16] proposed a sealed-cell infrared spectroscopy method in which prepolymer samples were dissolved and injected into a sealed IR cell. The absorbance of the —NCO band at 2270 cm^{-1} was used for rapid quantification of the isocyanate content. These approaches primarily focus on analyzing the —NCO in polyurethane prepolymers. However, when applied to one-shot synthesis systems, they require interrupting the reaction for offline sampling, which makes real-time monitoring impractical and cumbersome. To address this challenge, *in situ* spectroscopic techniques offer new possibilities for real-time monitoring of reaction progress. Wang *et al.*[17] monitored the thermal curing of polyurethane coatings using Fourier transform infrared (FTIR) spectroscopy to track the integrated absorbance of the —NCO band at 2273 cm^{-1} with internal standard calibration to quantify the conversion. Simultaneously, they analyzed the evolution of physical properties, such as hardness and glass transition temperature. Cimavilla-Román *et al.*[18,19] employed *in situ* FTIR to measure isocyanate conversion at different reaction stages, revealing the effects of catalysts, blowing agents, and silica aerogel fillers on the reaction kinetics of rigid polyurethane (RPU) foam. Elwell *et al.*[20,21] conducted a similar study on model flexible polyurethane systems using FTIR to track the attenuation of the 2270 cm^{-1} isocyanate peak with the aromatic C=C band at 1600 cm^{-1} as an internal standard. The isocyanate conversion data were cross-validated using adiabatic temperature rise experiments, and their results revealed a strong correlation between conversion degree and microphase-separated structural evolution during curing.

While these *in situ* FTIR techniques are effective for polyurethane systems with relatively low NCO content, they are less suitable for polyurethane grouting materials commonly used in grouting engineering applications. These systems typically contain high concentrations of isocyanate groups, leading to signal saturation and a "flat-top" phenomenon in the FTIR absorbance curve. As a result, the absorbance of the —NCO characteristic peak remained nearly constant throughout the reaction, preventing the accurate quantification of conversion rates and obscuring the true progression of chemical reactions, as shown in Fig. 1.

To overcome the limitations associated with the "flat-top" phenomenon in high —NCO systems, this study proposes a novel approach for the real-time quantification of component conversion during the expansion and curing process of

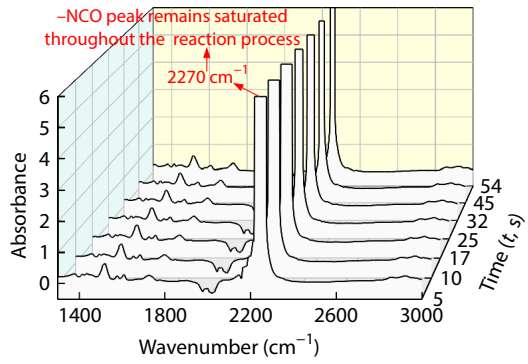

Fig. 1 Saturation of the —NCO absorption peak during the reaction process.

polyurethane grouting materials. Instead of directly monitoring the —NCO absorbance peak, this method employs the integrated absorbance of the C—O stretching vibration in the carbamate group (formed during the gelation reaction between isocyanate and polyol) as an indicator of polyol conversion. The absorbance was normalized using the C—H stretching peak as an internal standard to correct for potential fluctuations in the signal intensity. In parallel, the volume expansion of the reacting slurry was captured using LiDAR-based point cloud scanning. The gas volume generated during the reaction was estimated by reconstructing the three-dimensional morphology of the slurry surface at different time intervals. The conversion rate of the chemical blowing agent (*i.e.*, water) was calculated by combining the ideal gas law with the solubility-temperature curve of the physical blowing agent. With the conversion of polyol and water determined independently, the isocyanate conversion is inferred through stoichiometric relationships by considering that isocyanate is primarily consumed through two dominant pathways: gelation through the reaction between isocyanate groups and hydroxyl groups in the polyol, and foaming through the reaction between isocyanate groups and water, which produces carbon dioxide gas. It is also recognized that, under elevated-temperature conditions in polyurethane systems, a small fraction of isocyanate may be additionally consumed by secondary reactions (*e.g.*, formation of allophanate/biuret structures or isocyanate trimerization).[22] If such secondary consumption occurs, it will not affect the directly measured polyol conversion or the water conversion derived from gas generation, but it will influence the interpretation of the inferred isocyanate conversion. The stoichiometrically inferred value should therefore be regarded as an apparent and conservative estimate, meaning that the true isocyanate consumption may be slightly higher than the value calculated from the two dominant reactions alone. Notably, the extent of these secondary pathways is expected to be limited to the specific stage analyzed in this study. The present analysis targets the rapid expansion and curing window relevant to grouting applications; although the temperature can reach about 120 °C, the system simultaneously undergoes fast viscosity build-up and rapid network formation, which quickly reduces molecular mobility and restricts the diffusion-controlled encounters between residual —NCO groups and already-formed urethane/urea sites. As a result, gelation and foaming remain the dominant —NCO-consuming pathways

https://doi.org/10.1007/s10118-026-3604-y

during this short early time window, while the accumulation of allophanate/biuret linkages is expected to be minor. Therefore, the inferred isocyanate conversion remains a practical and information-rich metric for tracking reaction pathway evolution and for providing experimental inputs for kinetic parameter identification and process modeling.

This method was applied to a polyurethane polymer slurry used in practical engineering scenarios, yielding time-dependent conversion profiles for each reactive component. These data enabled a detailed analysis of the evolution of key reaction pathways within the polymer system. The proposed approach provides an experimental basis for determining the kinetic parameters of polyurethane grouting systems and modeling the reaction process, which is essential for elucidating the slurry diffusion mechanisms and guiding the optimization of field application parameters.

EXPERIMENTAL

Raw Materials and Reaction Mechanism

Materials

The polymer grouting material used in this study comprised two components: A and B, as shown in Fig. 2. Component A was polymeric methylene diphenyl diisocyanate (PAPI). Component B primarily consists of rigid foam polyether and polyester polyols (50 wt%), along with triethyl phosphate as a flame retardant (10 wt%), tertiary amine and metallic catalysts (2 wt%), physical blowing agents (5 wt%), chemical blowing agents with water as the active component (0.5 wt%), surfactants (0.5 wt%), and other auxiliary additives.

Chemical reaction principles

Upon mixing components A and B, chemical reactions are initiated promptly. The two primary reactions involved are polymerization (gelation) and foaming.[23] Polymerization occurs between the isocyanate (—NCO) groups and hydroxyl (—OH) groups of the polyols, resulting in the formation of polyurethane polymers. The chemical equation used is as follows:

$$R-NCO + R'-OH \rightarrow R-NH-\overset{\overset{O}{\|}}{C}-O-R' \quad (1)$$

The second reaction is the foaming reaction, in which isocyanate reacts with water and serves as a chemical blowing agent to form unstable carbamic acid, which subsequently decomposes into carbon dioxide and urea. The reaction equation is given below.[24,25]

$$2R-NCO + H_2O \rightarrow R-NH-\overset{\overset{O}{\|}}{C}-NH-R + CO_2\uparrow \quad (2)$$

Following mixing of the two components, initial microbubbles (gas nuclei) were formed. As the reactions proceed, substantial heat is continuously generated, leading to a gradual increase in the system temperature. Once the temperature surpasses the boiling point of the physical blowing agent, the dissolved liquid blowing agent vaporizes. Along with the carbon dioxide released from the chemical foaming reaction, these gases dispersed within the slurry as fine bubbles, thereby contributing to the progressive volumetric expansion of the grouting material.

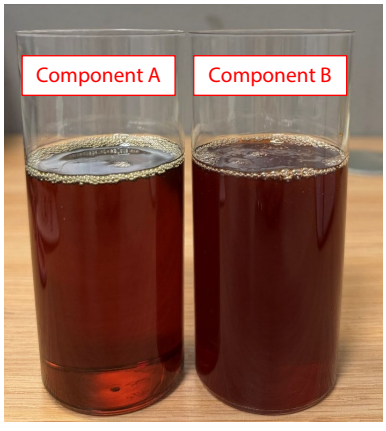

Fig. 2 Raw materials.

FTIR-based Monitoring of Hydroxyl Conversion

Instrument setup and data acquisition

The experiment employed a Fourier transform infrared spectrometer (FTIR, Thermo Scientific Nicolet iS50) equipped with a diamond attenuated total reflection (ATR) probe and an OMNIC™ data acquisition system. The instrument utilizes a Michelson interferometer to generate interference signals, which are detected in real time by a deuterated triglycine sulfate (DTGS) detector to monitor the characteristic infrared absorption bands of the sample (wavenumber range: 4000–650 cm^{-1}; resolution: 4 cm^{-1}). The ATR probe was composed of a high-temperature and corrosion-resistant diamond crystal. Based on the principle of attenuated total reflection, the infrared beam undergoes a single total internal reflection within the crystal, generating an evanescent wave that penetrates the surface layer of the sample (to a depth of approximately 0.5–2 μm). The absorption signal was then returned to the spectrometer and converted into a molecular vibrational spectrum *via* Fourier transformation. The conversion rate of the target compound was quantitatively determined by tracking the variation in the peak area corresponding to specific functional groups and correcting for signal fluctuation using an internal standard peak. The experimental setup is shown in Fig. 3.

Nucleophilic addition mechanism between isocyanate and polyol

During gelation, the electrophilic carbon atom in the isocyanate (—NCO) group undergoes nucleophilic attack by the hydroxyl (—OH) group. The lone pair of electrons on oxygen

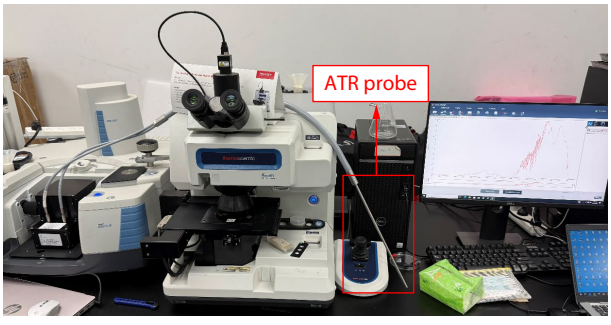

Fig. 3 In-line Fourier transform infrared (FTIR) spectrometer.

https://doi.org/10.1007/s10118-026-3604-y

forms a C—O bond with carbon, while a proton from the hydroxyl group is transferred to the nitrogen atom, resulting in the formation of an —NH group.[26] This reaction consumes one hydroxyl group and generates a urethane linkage containing a newly formed C—O bond, as illustrated in Fig. 4. Thus, the formation of C—O bonds serves as an indicator of the hydroxyl group conversion. Accordingly, the absorption band at 1225 cm^{-1}, corresponding to the C—O stretching vibration of the urethane (carbamate, —NH—COO—) linkage, was selected to monitor the reaction progress, and a closely located band at about 1226 cm^{-1} was assigned to the —NH—COO— structure in an independent polyurethane-related FTIR study.[27] It is recognized that the water isocyanate pathway may form urea/biuret-type species and introduce weak absorptions within the broader 1000–1300 cm^{-1} fingerprint region. However, the time-resolved ATR-FTIR data for a PAPI + water system show that the water-derived spectral response is distributed over multiple bands (including about 1231 and 1204 cm^{-1}), and that the most prominent diagnostic changes occur in the amide and carbonyl regions (*e.g.*, about 1638 and 1555 cm^{-1}), whereas the features in the vicinity of 1220–1250 cm^{-1} are comparatively less dominant.[28] Moreover, in the present formulation, the water dosage is very low relative to the polyol fraction, which intrinsically limits the maximum amount of urea/biuret structures that can form. Therefore, any overlap contribution in the 1186–1252 cm^{-1} integration window is expected to be minor and does not affect the applicability of the integrated band method adopted here. According to the literature, the asymmetric C—H stretching band at 2923 cm^{-1} (which remained constant during the reaction) was used as an internal reference band.[29] The conversion rate of polyol was then quantitatively analyzed by measuring the changes in the integrated absorbance of the C—O band relative to the internal reference.

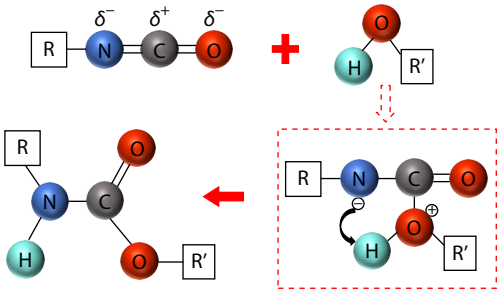

Fig. 4 Ionic rearrangement mechanism of isocyanate-polyol reaction.

Experimental procedure

The experimental procedure began with the pretreatment of the samples in a climate-controlled laboratory (RH: 35%±3%, 25±1 °C). Components A and B were separately preheated in a sealed thermostatic chamber at 28 °C for 30 min to minimize pre-reaction exposure to ambient moisture. After preheating, equal volumes of the two components were mixed and stirred for 5 s to ensure a uniform dispersion. The ATR probe was immediately immersed in the reaction mixture at a fixed position for the duration of measurement. Real-time FTIR data acquisition (resolution: 4 cm^{-1}) was initiated, and the probe was removed before gelation was complete. After the system was fully cured, the surface spectrum was re-measured using the ATR probe for the final calibration, enabling an accurate comparison of the reaction progress before and after curing. To ensure data reliability, each FTIR measurement was repeated thrice (n=3) under the same conditions, and the average values with standard deviations were reported.

Chemical Blowing Agent Conversion Rate Test

Physical blowing agent solubility test

Following the mixing of components A and B, water reacts with isocyanate to produce urea and carbon dioxide (CO_2). Under the combined influence of the generated CO_2 and vaporization of the physical blowing agent, the polymer slurry underwent rapid volumetric expansion. In this study, the water conversion rate was indirectly determined by quantifying the amount of CO_2 produced during the reaction. To eliminate interference from the physical blowing agent, component B was subjected to separate heating, and a solubility-temperature relationship was established based on the measured changes in the slurry volume and temperature. It is recognized that the effective solubility-temperature behavior of the physical blowing agent in the actual reacting A/B mixture may not be strictly identical to that in neat component B because introducing component A and the concurrent formation of polymer/urea structures can modify the medium (*e.g.*, polarity, viscosity, and evolving morphology). Nevertheless, using neat component B provides a reproducible and physically grounded calibration that captures the dominant temperature dependence of the physical blowing during the rapid expansion and curing window. Any deviation of the true solubility in the reacting mixture from the B-based calibration would primarily manifest as an uncertainty in partitioning the total gas volume into the physical-blowing contribution and chemically generated CO_2 contribution (*i.e.*, potential over- or under-estimation of CO_2). Importantly, this does not compromise the validity of the proposed approach, as it still enables a practical, time-resolved estimation of the CO_2 derived gas volume required for calculating water conversion, whereas the polyol conversion is obtained independently from FTIR and is unaffected by the solubility approximation. Moreover, because the present work focuses on the short, application-relevant expansion and curing stage where the temperature rises rapidly and viscosity builds up quickly, gelation and foaming dominate, and the B-based temperature-indexed calibration remains an effective approximation for separating physical blowing from chemical CO_2 generation.

The experimental setup, illustrated in Fig. 5, consisted of a temperature acquisition system, K-type thermocouple, and electromagnetic heating device. A 20 mL sample of component B was placed in a glass beaker, and the thermocouple was inserted into the slurry and connected to the data logger *via* a cable. After the setup was completed, the beaker was heated using an electromagnetic plate. As the temperature increased, the physical blowing agent began to vaporize, generating fine bubbles dispersed throughout the slurry and promoting its expansion. Throughout the heating process, the slurry temperature was continuously recorded in real time and the expansion behavior was simultaneously captured using a camera for further analysis. All experiments were repeated thrice to ensure the accuracy and reproducibility of the test results.

https://doi.org/10.1007/s10118-026-3604-y

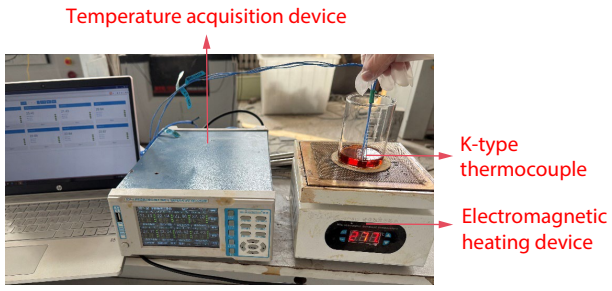

Fig. 5 Heating-vaporization device for physical blowing agent.

Temperature test during the reaction process

Components A and B were preheated to 28 °C, and 20 mL of each component was quickly mixed in a beaker. To monitor the temperature evolution and assess the potential spatial temperature gradients during the exothermic foaming reaction, three K-type thermocouples were suspended in the slurry at different radial positions at the same depth: geometric center (center), half-radius (1/2*R*), and near the inner wall (*R*=6 cm). The thermocouples were connected to a multichannel temperature data logger, which continuously recorded the slurry temperature as a function of time throughout the reaction process.

Three-dimensional reconstruction of slurry volume

(i) Scanning setup. To accurately measure the volume change of the slurry during the reaction process, a LiDAR Scanner (iPhone 16 Pro rear LiDAR Scanner) was employed to capture the real-time depth/point-cloud data of the slurry surface. iPhone LiDAR provides ToF-based near-infrared depth sensing, and depth frames are obtained *via* Apple's AR framework (ARKit) using the scene-depth/depth-map output (*e.g.*, sceneDepth/ARDepthData) and converted to 3D point clouds for reconstruction. The device was rigidly fixed above the beaker (Fig. 6) to avoid motion-induced artifacts. According to prior characterization, the LiDAR depth map is typically available on a 256 × 192 grid (about 49k depth points per frame), and the effective depth-map update rate is typically of the order of about 15 Hz, with reliable depth sensing reported within a phone-to-target distance of approximately 0.2–2.0 m. In our setup, the phone-to-surface distance was maintained within this range, and the depth stream was recorded continuously to capture the rapid expansion during the reaction.

Based on this point cloud information, a three-dimensional reconstruction of the slurry morphology was performed. The total slurry volume was calculated by summing the volumes of individual triangulated mesh units derived from the reconstructed surface geometry. The experimental setup is illustrated in Fig. 6, comprising a LiDAR scanner, cylindrical glass beaker, and high-definition camera. Before initiating the measurements, components A and B were preheated to 28 °C and mixed rapidly (20 mL each) in a cylindrical glass beaker to initiate the reaction. Immediately after mixing, the LiDAR scanner was activated to continuously record changes in the surface point cloud of the expanding slurry in real-time. Simultaneously, an external camera captured the visual footage of the morphological evolution of the slurry throughout the reaction process.

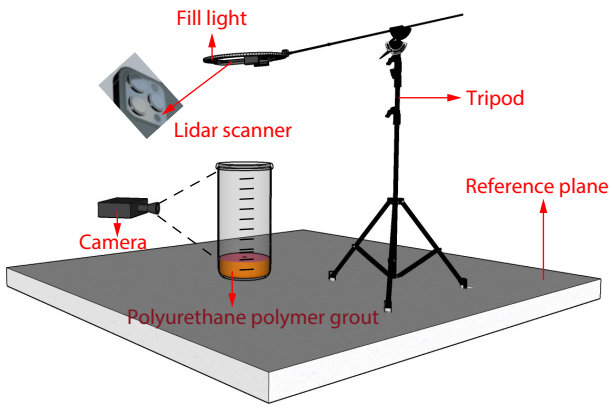

Fig. 6 Measurement device for volume changes of polymer slurry.

(ii) Volume measurement. Conventional methods typically approximate a curved surface formed by the expansion and curing of a polymer slurry as an ellipsoidal cap, as illustrated in Fig. 7. The volume of the slurry was then approximately calculated using the following formula.[30]

$$V(t) = \pi r^2 h(t) + \frac{2}{3}\pi r^2 [h_1(t) - h(t)] \quad (3)$$

where r is the radius of the cylindrical container, $h(t)$ is the height from the bottom of the container to the highest point of the slurry surface at time t, and $h_1(t)$ is the height of the cylindrical portion of slurry at time t.

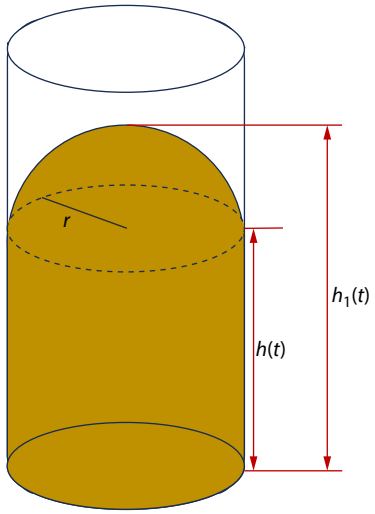

Fig. 7 Polymer slurry volume calculation diagram.

However, during the actual expansion of the slurry, the liquid surface did not instantly form an ideal ellipsoidal shape. Instead, it gradually bulges as the reaction proceeds, and the viscosity of the slurry increases, leading to significant errors in the volume estimation when using conventional methods. Furthermore, the liquid surface may become tilted or irregular during expansion, making accurate volume measurement even more challenging. To address these issues, LiDAR scanning technology was employed to capture the point cloud data of the slurry surface, enabling precise volume estimation through three-dimensional reconstruction. The specific procedure is as follows.

A LiDAR-equipped device was fixed above the beaker to continuously capture the point cloud data of both the liquid surface and surrounding ground. Using the ground plane as a

reference, rotational correction was applied to the point cloud data to align the ground points with the *XY* plane. The *Z*-values of the surface point cloud were interpreted as actual height values. The surface point cloud was projected onto the *XY* plane, and its convex hull boundary points were extracted. Constrained by the inner diameter of the container, least-squares circle fitting was performed to determine the outer boundary of the slurry surface, as shown in Fig. 8.

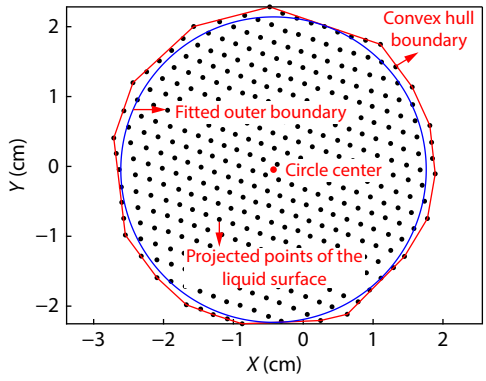

Fig. 8 Fitted outer boundary circle.

The Euclidean distance between each fitted outer boundary point and original surface point cloud was calculated. For each boundary point, the height of the nearest neighboring surface point was assigned as its corresponding parameter. To ensure smoothness of the reconstructed surface edge, cubic spline interpolation was applied to the regressed boundary points. The resulting liquid surface boundaries and corresponding surface points are shown in Fig. 9.

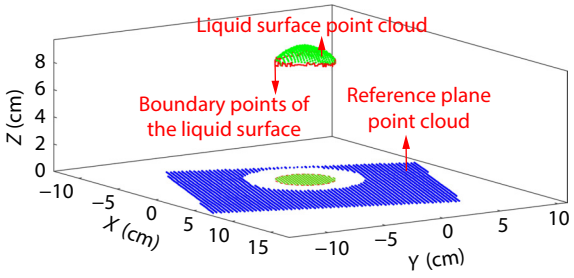

Fig. 9 Point cloud data of the liquid surface and ground level.

The three-dimensional point cloud of the liquid surface is triangulated into mesh elements. The vertices of each triangular mesh element are denoted by (x_{i1}, y_{i1}, z_{i1}), (x_{i2}, y_{i2}, z_{i2}), and (x_{i3}, y_{i3}, z_{i3}). The average height of the mesh vertices, denoted as z_{i1}, z_{i2} and z_{i3}, was considered as the height of the triangular prism. The projected area of the triangle on the horizontal plane was considered as the base area of the triangular prism. The total volume of the slurry is calculated by accumulating the volume of each triangular prism. The triangulated liquid surface point cloud is shown in Fig. 10.

Based on the liquid surface point cloud and the incorporation of the inner diameter and geometric features of the cylindrical glass beaker, a complete three-dimensional model was generated using a triangulation method. The formula for calculating the slurry volume is as follows.

$$V_{\text{total}} = \sum_{i=1}^{n} \left(S_i \cdot \frac{z_{i1} + z_{i2} + z_{i3}}{3} \right) \quad (4)$$

where S_i is the projected area of the i^{th} triangle on the *XY*-plane, and z_{i1}, z_{i2} and z_{i3} are the height values of the three corresponding three-dimensional vertices of the triangle.

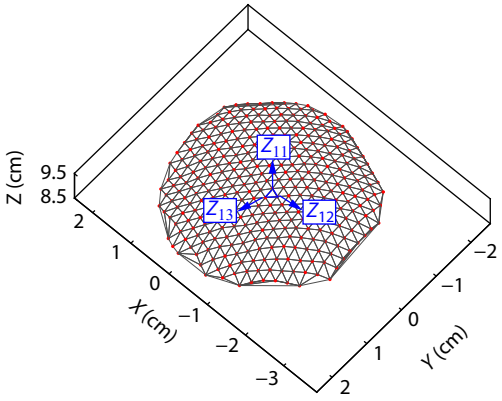

Fig. 10 Liquid level triangulation diagram.

RESULTS AND DISCUSSION

Evolution of Hydroxyl Conversion Rate

Spectral changes before and after reaction

Fig. 11 presents a comparison of infrared spectra before and after the polymerization reaction, with the corresponding changes in the absorbance integral area shown in Table 1. It is evident that the characteristic absorption peak for C—O bonds, observed between 1186 and 1252 cm^{-1}, significantly intensifies post-reaction. The absorbance integral area increased from 0.001 to 5.921, indicating the formation of urethane linkages during the reaction between the polyols and isocyanates. In contrast, the integral area of the C—H characteristic peak (2884–2955 cm^{-1}) remained relatively stable, with values of 1.936 before the reaction and 1.943 after the reaction, confirming the suitability and stability of this peak as an internal standard.

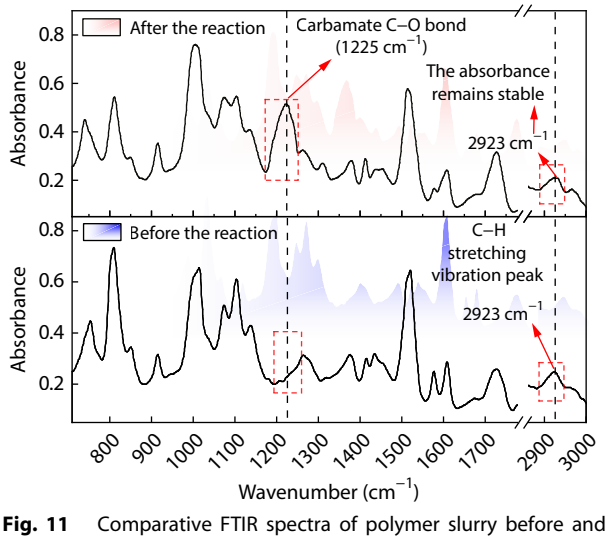

Fig. 11 Comparative FTIR spectra of polymer slurry before and after reaction.

Table 1 FTIR absorption band parameters of characteristic functional groups.

Functional group	Wavenumber (cm^{-1})	Time	Absorbance integral area
C—O Bond	1186–1252	Before reaction	0.001
		After reaction	5.921
C—H Bond	2884–2955	Before reaction	1.936
		After reaction	1.943

Spectral changes during the reaction

Fig. 12 illustrates the dynamic changes in the infrared spectra of the polymer slurry throughout the reaction. The characteristic absorption peak of C—O bonds (1225 cm^{-1}) gradually intensified as the reaction progressed, reflecting the formation of C—O bonds between polyols and isocyanates. In contrast, the characteristic C—H absorption peak (2923 cm^{-1}) remained stable throughout the reaction, showing no significant variation. Fig. 13 displays the temporal variation in the absorbance integral areas for the characteristic C—O and C—H peaks. Data represent the mean values of three independent experiments (n=3), and the error bars indicate the standard deviation. The change in the integral area, as opposed to the single peak height, provides a more accurate measure of C—O bond formation during the reaction by minimizing the influence of peak shape alterations and fluctuations in experimental conditions. The integral area of the C—O peak increased steadily over time, with a marked acceleration from 17 s to 45 s, indicating a higher reaction rate during this phase. This was followed by a slower increase, suggesting that the reaction rate decreased as the reaction continued.

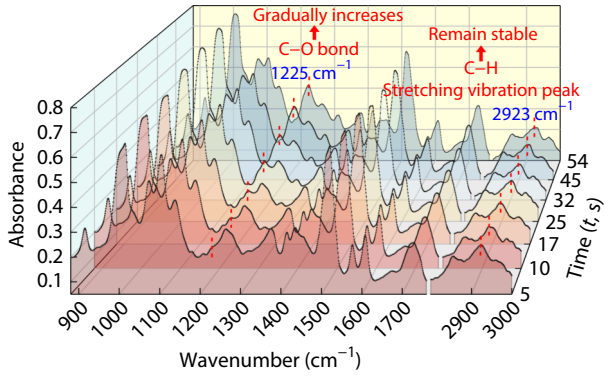

Fig. 12 Infrared spectral changes of the polymer during the reaction process.

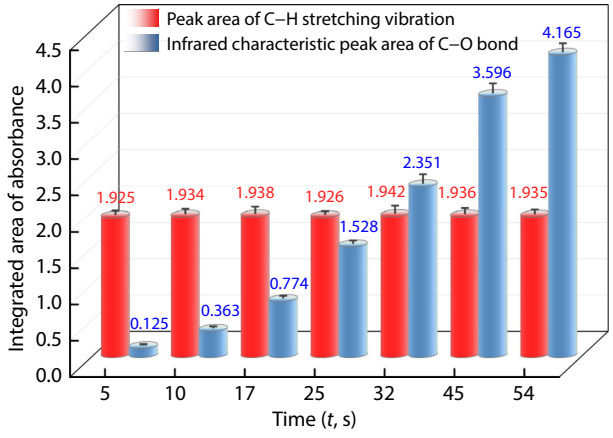

Fig. 13 Variation of characteristic peak integral area during the reaction process.

Conversion rate calculation

According to the Lambert-Beer law, absorbance is the product of the concentration of the absorbing substance, the molar absorption coefficient, and the path length. To eliminate the effects of path length fluctuations and baseline drift, the C—O characteristic peak was normalized using an internal standard characteristic peak. The calculation formula is as follows.[20]

$$X_{OH} = \frac{\left(\frac{A_{C\text{-}O,t}}{A_{C\text{-}H,t}} - \frac{A_{C\text{-}O,0}}{A_{C\text{-}H,0}}\right)}{\left(\frac{A_{C\text{-}O}}{A_{C\text{-}H}} - \frac{A_{C\text{-}O,0}}{A_{C\text{-}H,0}}\right)} \quad (5)$$

where $A_{C\text{-}O,t}$ is the integral area of the C—O characteristic peak at time t during the reaction, $A_{C\text{-}H,t}$ is the integral area of the C—H internal standard peak at time t, $A_{C\text{-}O,0}$ is the integral area of the C—O characteristic peak at the start of the reaction, $A_{C\text{-}H,0}$ is the integral area of the C—H internal standard peak at the start of the reaction, $A_{C\text{-}O}$ is the integral area of the C—O characteristic peak at the completion of the reaction, $A_{C\text{-}H}$ is the integral area of the C—H internal standard peak at the completion of the reaction.

$$r_{OH,t_i} = \frac{X_{OH,t_i} - X_{OH,t_{i-1}}}{t_i - t_{i-1}} \quad (6)$$

where r_{OH,t_i} is the rate of change of hydroxyl conversion at time t_i and X_{OH,t_i} is the hydroxyl conversion at time t_i calculated by Eq. (5); $X_{OH,t_{i-1}}$ is the hydroxyl conversion at the previous sampling time t_{i-1}; t_i, and t_{i-1} are two consecutive sampling times during the reaction. In this study, the initial condition was considered as $X_{OH,0}$=0.

The hydroxyl conversion rates at different time calculated using Eq. (5) are shown in Fig. 14. The conversion rate gradually increased as the reaction progressed. Based on the rate of change in conversion, the entire reaction process can be di-

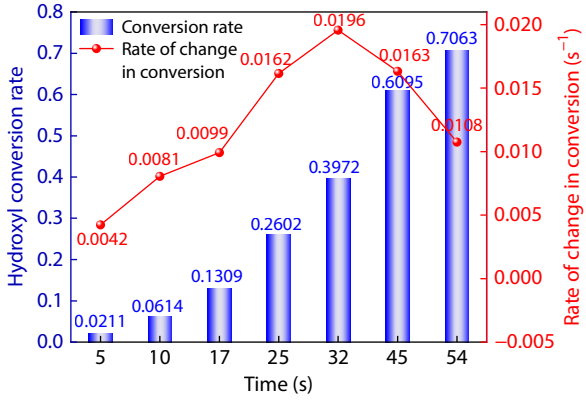

Fig. 14 Conversion rate of polyols at different time.

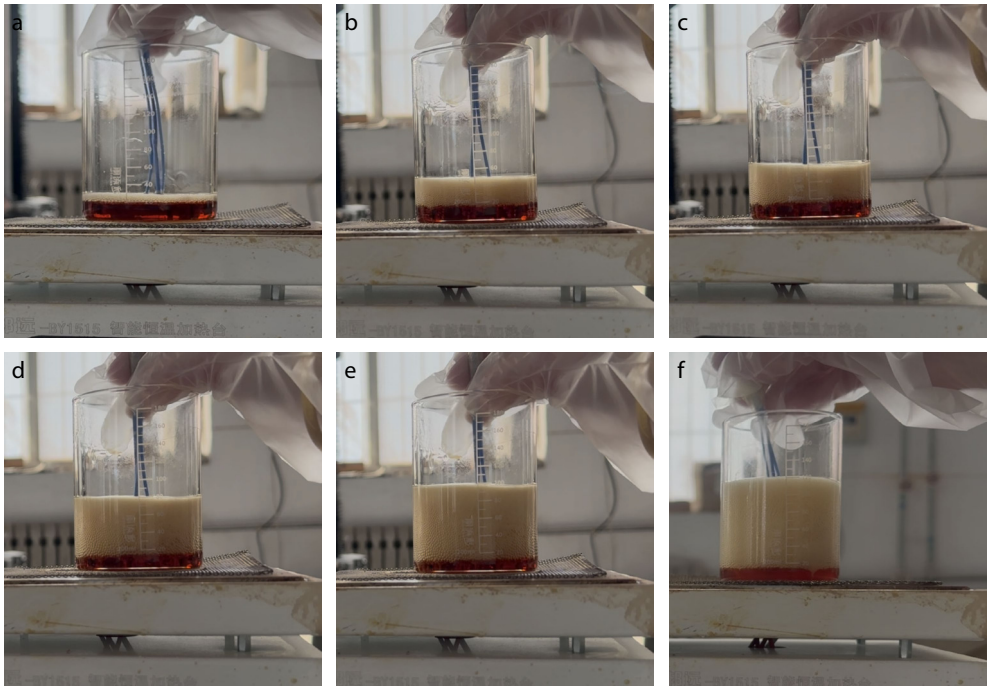

Fig. 15 Heating-induced expansion of component B: (a) 113.69 °C, (b) 134.92 °C, (c) 139.65 °C, (d) 144.62 °C, (e) 152.6 °C, (f) 190.23 °C.

vided into three stages. In the early stage (5–17 s), the hydroxyl conversion rate increases gradually from 0.0211 to 0.1309, with a relatively low growth rate. In the middle stage (17–45 s), the conversion rate increased rapidly from 0.1309 to 0.6095, maintaining a high rate of change in conversion. In the late stage (after 45 s), the rate of change in conversion begins to slow down, indicating that the reaction is gradually stabilizing.

Water Conversion from Carbon Dioxide Volume Estimation

Solubility curve fitting and equation

Because the liquid surface of component B remained at approximately the same level during heating, the height of the liquid was directly obtained by reading the graduation marks on the beaker (Fig. 15). The relationship between the slurry volume and temperature during the heating of component B is shown in Fig. 16. Based on the slurry volume expansion, the molar quantity of the vaporized blowing agent was calculated using the ideal gas law equation. Combining the initial parameters (the mass of the physical blowing agent m_B=1.08 g, the molar mass of the physical blowing agent M_B=116.9 g/mol, and the mass of Component B slurry m=21.6 g), the mass of the vaporized physical blowing agent at time t was calculated as $m_{BG}=n\times M_B$. The solubility of the physical blowing agent at time t was calculated using the formula: $r_{BL}=m_{BL}/m–m_B$. The results of the physical blowing agent solubility test and fitted curve are shown in Fig. 17. During the initial phase, the solubility of the physical blowing agent gradually decreased with increasing temperature. Above approximately 100 °C, the solubility of the physical blowing agent began to decrease more rapidly.

The fitting equation for the solubility of the physical blowing agent as a function of the temperature T is expressed as follows:

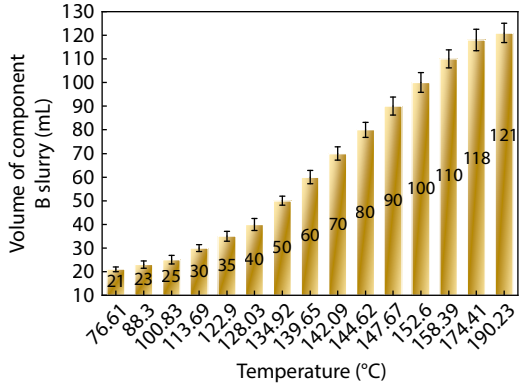

Fig. 16 Volume changes of component B slurry with temperature.

$$r_{BL} = a + (b - a) / (1 + \exp((T - 140.7) / c)) \quad (7)$$

where a=0.03654, b=0.05195, and c=7.897.

Water conversion calculation

(i) Temperature changes during the reaction process. Prior to mixing, Components A and B were preheated to 28 °C, and equal volumes (20 mL each) were rapidly mixed to initiate the reaction. The temperature evolution of the reacting slurry is shown in Fig. 18(a) and reported as the mean ± standard deviation from three independent experiments (n=3). To evaluate potential spatial temperature gradients, three K-type thermocouples were positioned at the same depth but at different radial locations (center, 1/2R, and near-wall R), and the corresponding comparison is shown in Fig. 18(b).

As shown in Fig. 18(a), the slurry temperature increased continuously and reached a peaked at approximately 120 °C. The temperature increased gradually at the beginning of the reaction and increased more rapidly between 20 and 60 s, reflecting the exothermic nature of the foaming/gelation reac-

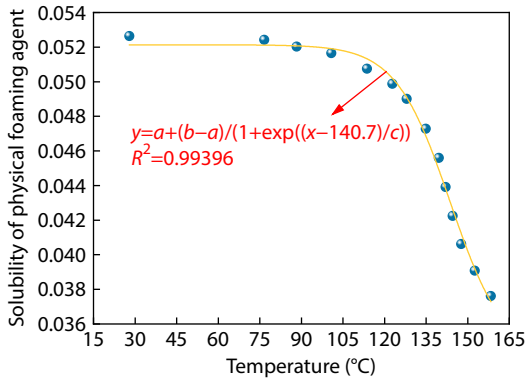

Fig. 17 Solubility test and fitting results of the physical foaming agent.

tions. After approximately 100 s, the temperature rise slowed and approached a plateau, indicating that the main reactions had largely proceeded, and the system approached thermal equilibrium. Fig. 18(b) further shows that the temperatures measured at different radial positions were very similar throughout the process, with a maximum difference of ≤ 4 °C.

(ii) Water conversion analysis of slurry. The morphology of the slurry during the free expansion process is shown in Fig. 19, and the reconstructed 3D shape of the slurry is presented in Fig. 20. As observed, the reconstructed surface closely matches the actual slurry profile.

Based on the solubility curve of the physical blowing agent, the contribution of its vaporization to the measured expansion volume was corrected, and the molar amount of carbon dioxide *n* was subsequently calculated using the ideal gas law (Eq. 8). Because polyurethane reactions are sensitive to moisture, particular attention was paid to experimental humidity conditions. All measurements were performed under monitored laboratory conditions, with the ambient relative humidity maintained at approximately 35%±3%. Under this controlled humidity level, the potential influence of atmospheric moisture on the calculated water conversion was expected to be minimal. This is further supported by the rapid reaction kinetics, where substantial expansion is completed within 60 s and the relatively small surface-to-volume ratio of the sample, which together limit the diffusion of external water vapor compared with the 0.5 wt% water intentionally added as the chemical blowing agent. Moreover, the elevated internal pressure and temperature (about 120 °C) during foaming further suppressed the infiltration of external moisture during the critical measurement period.

In addition, the spatial temperature nonuniformity was evaluated using three K-type thermocouples placed at the same depth but with different radial positions (center, 1/2*R*, and near-wall *R*). The results (Fig. 18b) showed that the radial temperature difference remained small throughout the reaction, with a maximum deviation of ≤4 K. To illustrate the resulting influence on the CO_2 molar calculation, a sensitivity example was provided at 45 s, where the measured temperature was 342.08 K (Table 2). If a conservative temperature deviation of ±5 K is assumed, the calculated *n* would change by only approximately ±1.5% (because *n* scales inversely with

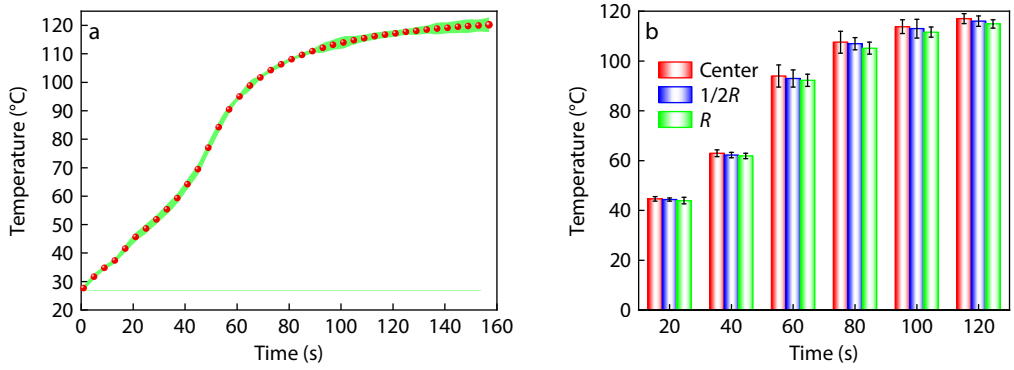

Fig. 18 Temperature evolution and spatial distribution during the foaming reaction. (a) Temperature-time profile of the reacting slurry; (b) Temperatures measured at different radial positions (center, 1/2*R*, and *R*).

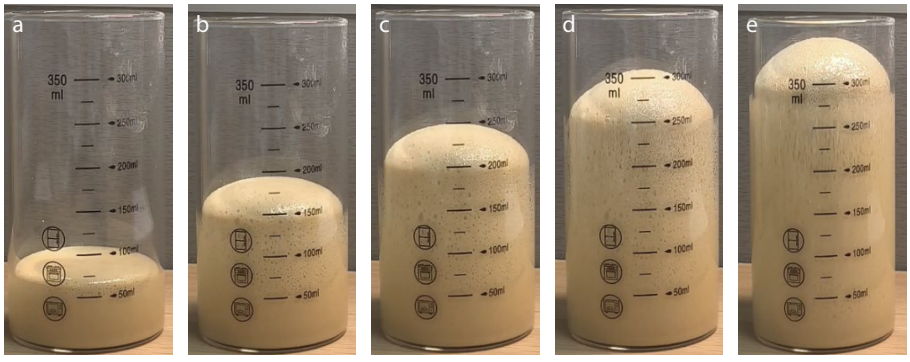

Fig. 19 Shape of the slurry during free expansion: (a) 17 s, (b) 32 s, (c) 45 s, (d) 58 s, (e) 81 s.

https://doi.org/10.1007/s10118-026-3604-y

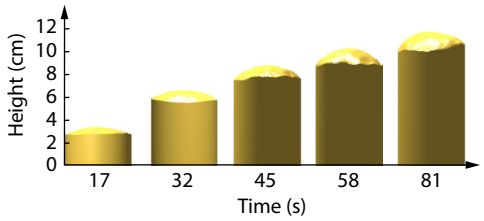

Fig. 20 3D reconstructed morphology of the slurry.

Table 2 Parameter variations during the reaction process.

Time (s)	V_{total} (mL)	T (K)	V_{141b} (mL)	V_{CO_2} (mL)	n (mol)
0	40.00	301.98	0	0	0
17	71.30	314.08	0	31.30	0.00121
32	153.80	327.51	0	113.80	0.00423
45	215.60	342.08	1.00	174.60	0.00622
58	276.41	364.60	2.30	234.11	0.00782
81	318.17	381.70	6.95	271.22	0.00863

the temperature under the ideal gas relationship). Therefore, the uncertainty introduced by the radial temperature gradient was minor. Based on these observations, the center temperature was used as the representative temperature in the calculation of n and subsequent water conversion.

The calculated parameters are summarized in Table 2 as mean values of three independent experiments (n=3).

$$p\Delta V(t) = nRT(t) \quad (8)$$

where P represents the standard atmospheric pressure (101.325 kPa), and R is the universal gas constant (8.314 J/(mol·k)).

Based on the stoichiometric equation of the isocyanate-water foaming reaction, the water conversion rate was determined by comparing the amount of carbon dioxide generated during the reaction with the initial molar amount of water. The calculated results are shown in Fig. 21. As illustrated, the water conversion rate progressively increased over time. Before 17 s, the conversion rate slowly increased. Between 17 and 32 s, the conversion rate increased rapidly from 0.1319 to 0.4603, reaching the maximum rate of change in the conversion rate. After 32 s, the rate of change of the conversion rate began to decrease, and the growth of the conversion rate gradually stabilized. From 58 s to 81 s, the rate of change was minimal and the water conversion rate gradually stabilized, finally reaching 0.9383 at 81 s.

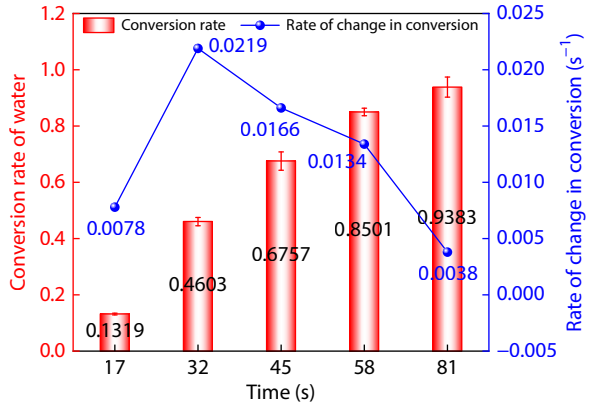

Fig. 21 Water conversion rate during reaction.

It should be noted that the water conversion calculated using Eq. (8) implicitly assumes complete gas retention, that is, all generated CO_2 remains in the slurry and contributes to the measured volume expansion. In practice, a small amount of CO_2 may escape, particularly during the early liquid-like stage before substantial viscosity build-up, which would cause the calculated water conversion to be a conservative (lower-bound) estimate. To quantify the potential magnitude of this systematic underestimation, we performed a sensitivity analysis by assuming gas retention efficiencies of 0.90, 0.95, and 1.00. Under a representative case of 0.95 retention, the water conversion increased from 0.1319 to 0.1388 (17 s), 0.4603 to 0.4845 (32 s), and 0.6757 to 0.7113 (45 s). These results indicate that a plausible minor gas loss would cause only small changes in the water conversion values; therefore, the η=1 assumption provides a conservative estimate, and the possible underestimation due to gas escape is expected to be limited.

(iii) Comparison of gelling and foaming reaction rates. A comparison with the hydroxyl conversion rate revealed that the water conversion rate remained consistently higher at all time points, indicating that the foaming reaction proceeded faster than the gelling reaction. This difference is mainly due to the following reasons: In the water isocyanate pathway, —NCO reacts with water to form an unstable carbamic acid intermediate that rapidly decomposes to CO_2 and a primary amine; the amine then reacts with —NCO to form urea linkages. Because amines are generally more reactive toward isocyanates than alcohols, the urea-forming step is intrinsically fast.[31] In contrast, gelling proceeds *via* the addition of —OH to —NCO to form urethane linkages, which is typically slower than amine-isocyanate chemistry. In addition, water, as a small and highly mobile molecule, can access —NCO sites efficiently at early times, whereas as the reaction proceeds, the viscosity increases and chain mobility decreases, making the polyol-isocyanate reaction more susceptible to diffusion limitations.[19] Consequently, the apparent gelling rate was increasingly hindered relative to blowing as the conversion increased.

CONCLUSIONS

For the commonly used self-expanding polyurethane polymer grouting materials in engineering, a high isocyanate group concentration causes the characteristic absorption peaks to remain saturated during testing, resulting in a "flat-top" phenomenon in the absorbance curve. This prevents accurate acquisition of the conversion rate over time through online infrared spectroscopy monitoring. To address this issue, a method for real-time measurement of the component reaction conversion rates of a polymer slurry is proposed, integrating Fourier-transform online infrared spectroscopy and three-dimensional point cloud reconstruction technologies. The method selects the C—O bond of carbamate, a gel reaction product, as the monitoring feature peak and combines internal standard correction methods for quantitative analysis of hydroxyl conversion rates. Laser radar point cloud scanning and three-dimensional reconstruction technologies were used to accurately measure the expansion volume of the slurry. By combining the ideal gas law and physical blowing agent solubility curve, the conversion of the chemical blowing agent participating in the foaming reaction was calculated to determine its conversion rate. The isocyanate conversion rate was indirectly calculated based on the mea-

sured polyol and chemical blowing agent conversion rates.

This method was used to monitor the component conversion rates of a commonly used polyurethane polymer grouting material throughout the reaction process. The results show that as the reaction progresses, the conversion rates of all slurry components exhibit a three-phase evolution pattern: in the early stage, the conversion rate increases slowly with a low rate of change in the conversion rate; during the mid-stage, the conversion rate rises rapidly, maintaining a high rate of change, and reaching its maximum rate of change in the conversion rate; in the final stage, the rate of change in the conversion rate gradually decreases, and the reaction stabilizes until completion. At all time points, the chemical blowing agent conversion rate was consistently higher than the hydroxyl conversion rate, indicating that the foaming reaction rate was generally faster than the gelation reaction rate during the chemical reaction process of the polymer slurry.

The proposed approach provides an experimental basis for identifying the kinetic parameters of chemical reactions in polyurethane polymer grouting materials and analyzing the reaction process of the slurry. It also lays the foundation for investigating slurry diffusion mechanisms and optimizing construction parameters.

Conflict of Interests

The authors declare no interest conflict.

Data Availability Statement

The data supporting the findings of this study are available from the corresponding author upon reasonable request.

ACKNOWLEDGMENTS

This work was financially supported by the National Natural Science Foundation of China (No. 52178401), Science and Technology Innovation Team Support Program for Henan Universities (No. 23IRTSTHN014), Natural Science Foundation of Henan Province of China (No. 252300421251), National Natural Science Foundation of China (Nos. 52578540 and 52478477), and the Cross-disciplinary Innovation Research Group Project of the Natural Science Foundation of Henan Province (No. 252300421827).

Graphical Abstract

Real-Time Monitoring of Component Conversion during the Foaming and Curing Process of Self-expanding Polyurethane Grouts

Xiao-Long Li, Xuan-Xuan Zi, Xiao-Feng Liu, Ming Guo, Yan-Hui Zhong, and Bei Zhang

Zhengzhou University

A real-time approach quantifies polyol, water, and apparent isocyanate conversions in high —NCO polyurethane grouts by ATR-FTIR (carbamate C—O) and LiDAR volume tracking, revealing three-stage kinetics with faster foaming than gelation.

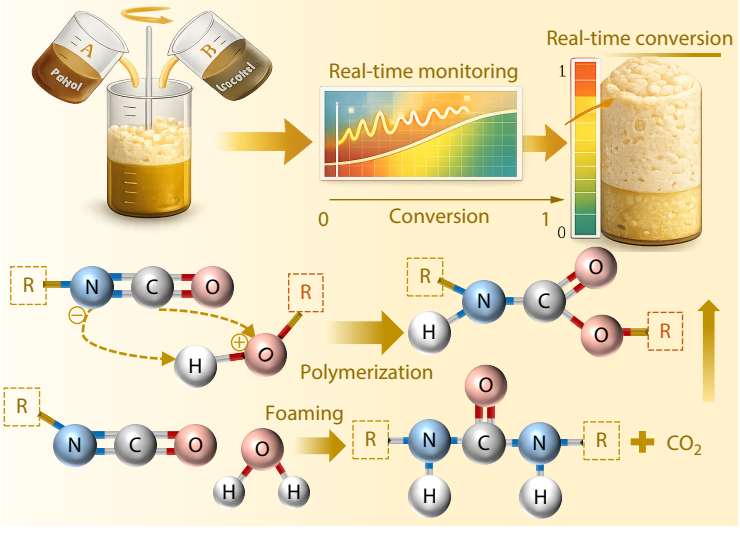

Chinese J. Polym. Sci. 2026, 44, 1843–1854 *https://doi.org/10.1007/s10118-026-3604-y*

REFERENCES

1 Zhang, L.; Wen, P.; Wang, Z.; Di, S.; Yin, W. Research progress on nonexcavation grouting reinforcement materials for roadways. *Mater. Rev.* **2017**, *31*, 98–105.
2 Wu, Y.; Zheng, Z.; Huang, Y.; Yan, L.; Du, X.; Jiang, J.; Liu, T. Integrated maintenance technology for rapid detection and trenchless reinforcement of heavy-duty pavement. *Constr. Eng.* **2020**, *42*, 2328–2330,2338.
3 Guo, C.; Cui, C.; Wang, F. Case study on treatment of voids under airport pavement by polymer grouting. *J. Mater. Civ. Eng.* **2020**, *32*, 05020006.
4 Wang, F.; Li, J.; Shi, M.; Guo, C. Research and application of new technologies for dam seepage control and reinforcement. *J. Hydroelectr. Eng.* **2016**, *35*, 1–11.
5 Lipshitz, S. D.; Macosko, C. W. Kinetics and energetics of a fast polyurethane cure. *J. Appl. Polym. Sci.* **1977**, *21*, 2029–2039.
6 Kamal, M. R. Thermoset characterization for moldability analysis. *Polym. Eng. Sci.* **1974**, *14*, 231–239.
7 Dimier, F.; Sbirrazzuoli, N.; Vergnes, B.; Vincent, M. Curing kinetics and chemorheological analysis of polyurethane formation. *Polym. Eng. Sci.* **2004**, *44*, 518–527.
8 Li, X.; Chen, C.; Jia, H.; Ma, P.; Gui, Y.; Zhang, B.; Zhong, Y. Experimental and numerical study on expansion mechanism of polyurethane grout considering chemical reactions. *J. Railw. Sci. Eng.* **2023**, *20*, 4163–4173.
9 Li, X.; Zhao, Z.; Chen, K.; Ma, P.; Chen, C.; Zhong, Y.; Zhang, B. Simulation study on compaction-splitting grouting of polymer considering chemical reactions. *Rock Soil Mech.* **2024**, *45*, 2823–2838.
10 Qian, J.; Liu, S.; Li, X.; Jin, J.; Wang, X.; Xue, S. Research progress on detection methods of isocyanate group content in the polyurethane industry. *Contemp. Chem. Ind.* **2015**, *44*, 2928–2930.
11 Kong, D.; Liu, C.; Ma, L.; Zhang, D.; Li, Y. Improved potentiometric titration method for determining isocyanate groups in PAPI. *Chem. Chem. Eng. Manag.* **2021**, *34*, 52–53,73.
12 Lv, J.; Su, H.; Yao, Z.; Li, Z.; Yan, Y.; Sun, Z. Online monitoring of —NCO content in polyurethane prepolymer using Raman spectroscopy. *Coat. Ind.* **2015**, *45*, 57–60,66.
13 Wang, Y.; Zhang, H.; Duan, C. Advances in detection methods and technology applications for low free isocyanates. *Polyurethane Ind.* **2023**, *38*, 5–9.
14 HG/T 2409-1992 Determination of isocyanate group content in polyurethane prepolymer. Ministry of Chemical Industry of the People's Republic of China, Beijing, China, **1992**.
15 Chen, W.; Wang, X.; Huang, Z. Determination of free diisocyanates in IPDI- and MDI-type polyurethane prepolymers. *Polyurethane Ind.* **2009**, *24*, 43–46.
16 Wu, M.; Du, Y.; Yang, Y.; Wang, G.; Yao, Z.; Gao, S. Determination of isocyanate group content in polyurethane prepolymers by infrared spectroscopy. *Coat. Ind.* **2010**, *40*, 69–72.
17 Wang, T.; Segura, J. J.; Graversen, E.; Weinell, C. E.; Dam-Johansen, K.; Kiil, S. Simultaneous tracking of hardness, reactant conversion, solid concentration, and glass transition temperature in thermoset polyurethane coatings. *J. Coat. Technol. Res.* **2021**, *18*, 349–359.
18 Cimavilla-Román, P.; Pérez-Tamarit, S.; Santiago-Calvo, M.; Rodríguez-Pérez, M. A. Influence of silica aerogel particles on the foaming process and cellular structure of rigid polyurethane foams. *Eur. Polym. J.* **2020**, *135*, 109884.
19 Cimavilla-Román, P.; Santiago-Calvo, M.; Rodríguez-Pérez, M. Dynamic mechanical analysis during polyurethane foaming: relationship between modulus build-up and reaction kinetics. *Polym. Test.* **2021**, *103*, 107336.
20 Elwell, M. J.; Ryan, A. J.; Grünbauer, H. J. M.; Van Lieshout, H. C. FT i.r. study of reaction kinetics and structure development in model flexible polyurethane foam systems. *Polymer* **1996**, *37*, 1353–1361.
21 Elwell, M. J.; Ryan, A. J.; Grünbauer, H. J. M.; Van Lieshout, H. C. *In situ* studies of structure development during the reactive processing of model flexible polyurethane foam systems using FT-IR spectroscopy, synchrotron SAXS, and rheology. *Macromolecules* **1996**, *29*, 2960–2969.
22 Liu, Z.; Fang, Z.; Zheng, N.; Yang, K.; Sun, Z.; Li, S.; Li, W.; Wu, J.; Xie, T. Chemical upcycling of commodity thermoset polyurethane foams toward high-performance 3D photo-printing resins. *Nat. Chem.* **2023**, *15*, 1773–1779.
23 Demir, M. M.; Yilgor, I.; Yilgor, E.; Erman, B. Electrospinning of polyurethane fibers. *Polymer* **2002**, *43*, 3303–3309.
24 Baser, S. A.; Khakhar, D. V. Modeling of the dynamics of R-11 blown polyurethane foam formation. *Polym. Eng. Sci.* **1994**, *34*, 632–641.
25 Baser, S. A.; Khakhar, D. V. Modeling of the dynamics of water and R-11 blown polyurethane foam formation. *Polym. Eng. Sci.* **1994**, *34*, 642–649.
26 Gertig, C.; Erdkamp, E.; Ernst, A.; Hemprich, C.; Kröger, L. C.; Langanke, J.; Bardow, A.; Leonhard, K. Reaction mechanisms and rate constants of auto-catalytic urethane formation and cleavage reactions. *Chem. Open* **2021**, *10*, 534–544.
27 Ma, Y.; Jiang, Y.; Tan, H.; Zhang, Y.; Gu, J. Rapid and Efficient Route to Preparation of Isocyanate Microcapsules. *Polymers* **2017**, *9*, 274.
28 Haupt, R. A. Structural determination of copolymers from the cross-catalyzed reactions of phenol–formaldehyde and polymeric methylene diphenyl diisocyanate. Thesis, Virginia Polytechnic Institute and State University, Blacksburg, VA, USA, **2013**.
29 Santiago-Calvo, M.; Tirado-Mediavilla, J.; Ruiz-Herrero, J. L.; Rodríguez-Pérez, M. A.; Villafañe, F. Effects of functional nanofillers on reaction kinetics, microstructure, and thermal and mechanical properties of water-blown rigid polyurethane foams. *Polymer* **2018**, *150*, 138–149.
30 I. E. Ireka, D. Niedziela, K. Schaefer, J. Troeltzsch, K. Steiner, F. Helbig, T. Chinyoka, L. Kroll, Computational modeling of the complex dynamics of chemically blown polyurethane foam. *Phys. Fluids* **2015**, *27*, 113102.
31 Stern T. Chemical structure and side reactions in polyurea synthesized *via* the water-diisocyanate synthesis pathway. *Polymers* **2023**, *15*, 3524.

https://doi.org/10.1007/s10118-026-3604-y